NUCLEOSYNTHESIS IN NEUTRON RICH SUPERNOVA EJECTA

MICHAEL D. DELANO
Belfer Graduate School of Science, Yeshiva University, New York, N.Y., U.S.A.

and

A. G. W. CAMERON
Belfer Graduate School of Science, Yeshiva University, New York, N.Y., U.S.A.

and

Institute for Space Studies, Goddard Space Flight Center, NASA, New York, N.Y., U.S.A.

(Received 21 May; in final form 21 July, 1970)

Abstract. A nuclear reaction network of 903 different, strong and electromagnetic reactions, linking 107 chemical constituents is used to study the elements synthesized in the neutron rich material, ejected in supernova explosions. A large number of three body reactions virtually eliminates the usual bottle neck at the $A = 5$ mass gap.

For initially high temperatures and densities, $T = 10^{10}$ K and $\varrho = 7 \times 10^8$ gm/cm^3, with expansion time scales of 10^{-3}–10^{-2} sec, three different n to p ratios, $n/p = 4$, $n/p = \frac{3}{2}$, and $n/p \sim 1$, are considered for the ejected matter. In all three cases, the material synthesized is preponderantly heavy. For the $n/p = 4$ model, the conditions at the charged particle freeze-out are ideal for the 'r-process'. The onset of this rapid neutron capture phase is explicitly shown with a sequence of time lapse abundance plots.

1. Introduction

Recent observational work, locating pulsars at the sites of supernova remnants, along with theoretical arguments suggesting the identification of neutron stars with pulsars, have emphasized the importance of having reliable models for supernova explosions. However, supernova calculations, with little observational data to guide them, have proceeded mainly along theoretical lines. As a consequence they have been plagued by many uncertainties and contradictions. One of these is the apparent disparity between the amount and rate of supernova ejected mass in the galaxy and the observed solar system abundances of the heavy chemical elements (Truran *et al.*, 1968).

The present work is an in depth study of the elements synthesized by thermonuclear reactions in these explosions. The preliminary investigations of Truran *et al.* (1968), which studied supernova nucleosynthesis with a bare skeleton chain of (n, ν) and (α, γ) reactions, suggested that the physical conditions in current models would favor a break through past carbon to the heavier elements. With a complete network of reactions up through the silicon isotopes and a bare (n, γ) and (α, γ) extension network from silicon to the nickel isotopes, we confirm this and are able to give some estimates for the time scales involved. Furthermore, the observation of Truran *et al.* (1968), that the rapid neutron capture process of heavy element production will occur in these models, is actually seen to be underway at the termination of one of the presented calculations.

Astrophysics and Space Science **10** (1971) 203–226.

We also find that the lightest elements, Li, Be and B, stand very little chance of surviving these model explosions. Some limits on the explosive conditions that might produce them are given.

While no attempt has been made here to resolve the discrepancy between these models and the heavy element abundances, recent work by Colgate (1970), indicates that the calculated amount of neutron rich ejecta, in these explosions, is an overestimate, thus making them more compatible with observation.

In Section 2 a brief discussion of the hydrodynamic calculations for supernova explosions, summarizes the work of Colgate and White (1966), Arnett (1966, 1967) and Schwartz (1967). Section 3 presents the nuclear reactions linking the 107 nuclei considered. This is accomplished by a series of graphical displays called network diagrams, the construction of which are detailed in a set of formal rules. Emphasizing the importance of three body reactions in bridging the mass gap at $A=5$, the overall reliability of the network is also briefly touched upon. The nucleosynthesis products for the three n to p ratios, $n/p=4$, $n/p=\frac{3}{2}$, and $n/p\sim 1$, are given in Section 4 and the time scales for the establishment of nuclear statistical equilibrium are examined. In Section 5, the conditions most favorable to the onset of the r-process are investigated. They are compared with those suggested by other workers. The appendix presents the numerical techniques used to integrate the network equations.

2. The Supernova Model

Studied in detail by Colgate and White (1966), Arnett (1966, 1967) and Schwartz (1967), the hydrodynamic models for supernova explosions have encountered computational difficulties in handling neutrino transport properties (Colgate, 1968; and Arnett, 1968). These models investigated the behavior of highly evolved massive stars, undergoing gravitational collapse. The supporting pressure of the initial configuration was removed either by the decrease in the thermal photon pressure due to the photodisintegration of nuclei or by the decrease in degeneracy pressure, resulting from the capture of high Fermi energy electrons on nuclei.

Essentially free falling onto itself, the stellar material is compressed to enormously high temperatures ($\sim 10^{11}$–10^{12} K) and densities ($\sim 10^{14}$ gm/cm^3) in the central regions. A hot, dense core of degenerate neutrons is formed, with the envelope of the star still raining down on it. Opaque to all forms of radiation, this neutron core radiates away its thermal energy as a black body neutrino emitter, with an energy flux of $\sim 10^{54}$ erg/sec at its surface. These neutrinos will be absorbed by, and consequently will heat up, the colder exterior mass, which has not yet fallen to nuclear densities. Some of the details of the fate of the still infalling material are in dispute (Colgate, 1968; Arnett, 1968).

The formation of a strong shock front in the models of Colgate and White (1966) and the weak to none in those of Arnett (1966, 1967) are primarily due to different methods in treating the deposition of the neutrino energy in the stellar envelope. The important point in either case, however, is that the outer layers of the star are

not ejected by a shock wave propagating radially outward from the core (Schwartz, 1966). The material, collapsing inward, is heated up by compression and by the absorption of the core neutrinos. In the neighborhood of the core, the pressure builds up to the point where this inward motion is halted ('core bounce') and the material begins to expand outward, hydrodynamically, converting its internal energy into kinetic energy of mass motion. Some of it escapes the star and is to be identified with the ejected gases of a supernova explosion.

Recently, one of us (Delano, 1969) calculated that the momentum carried by the core neutrinos will create a radially outward pressure on the innermost zones, exterior to the core, sufficient, at least temporarily, to completely reverse their inward motion. Colgate, in a reevaluation of the problem (1970), has found that some, if not all, of this material will fall back onto the core after the neutrino flux from the core gives out. These zones, processed to such high temperatures and densities that they are composed of unbound nucleons, are the most active ones for element synthesis by thermonuclear reactions. While it is clearly uncertain how much of the material escapes the star, the manner in which it does is not in dispute. Therefore, we have chosen to study nucleosynthesis in an interior mass zone, in a $2\,M_{\odot}$ supernova model of Arnett (1967), as it expands and cools, while leaving the star.

The calculation begins when the gas, composed of nondegenerate neutrons and protons, has cooled to 10^{10} K and has a density of 7×10^{8} gm/cm^3. Just prior to this, at $T\sim2\times10^{10}$ K and $\varrho\cong7\times10^{9}$ gm/cm^3, the weak interactions froze out and determined the ratio of neutrons to protons; which Arnett (1967) estimates to be $n/p\sim8$. This estimate is not at all definite and we have selected a middle ground between it and equal numbers of neutrons and protons, by studying nucleosynthesis, under the above conditions, for the three cases $n/p=4$, $n/p=\frac{3}{2}$, and $n/p\sim1$ (51% neutrons and 49% protons). Noting that the expansion is adiabatic, the temperature and density profiles (time histories) are shown in Figure 1. The expansion time scale is between 10^{-3} and 10^{-2} sec. From 10^{-2} to 10^{-1} sec the temperature decreases to the point where the charged particles in the gas are no longer energetic enough to overcome their mutual coulomb barriers, thus ending nuclear reactions among charged particles. For this reason, it is called the 'charged particle freeze out'.

The elements present, after the charged particle freeze out, can still undergo significant nuclear transmutation by neutron capture and β decay. Depending on the amount of free neutrons and the temperature and density at freeze out, any material heavier than He, may be processed to higher mass numbers by the rapid capture of these neutrons while successive β decays increases its atomic number. In short, studying the products of thermonuclear reactions among charged particles will answer the question of whether the *r*-process nuclei could have been manufactured in supernova explosions.

3. The Nuclear Reaction Network

The basic incredients in any nucleosynthesis problem are a selection of chemical elements and a set of nuclear reactions which transmute one species into another.

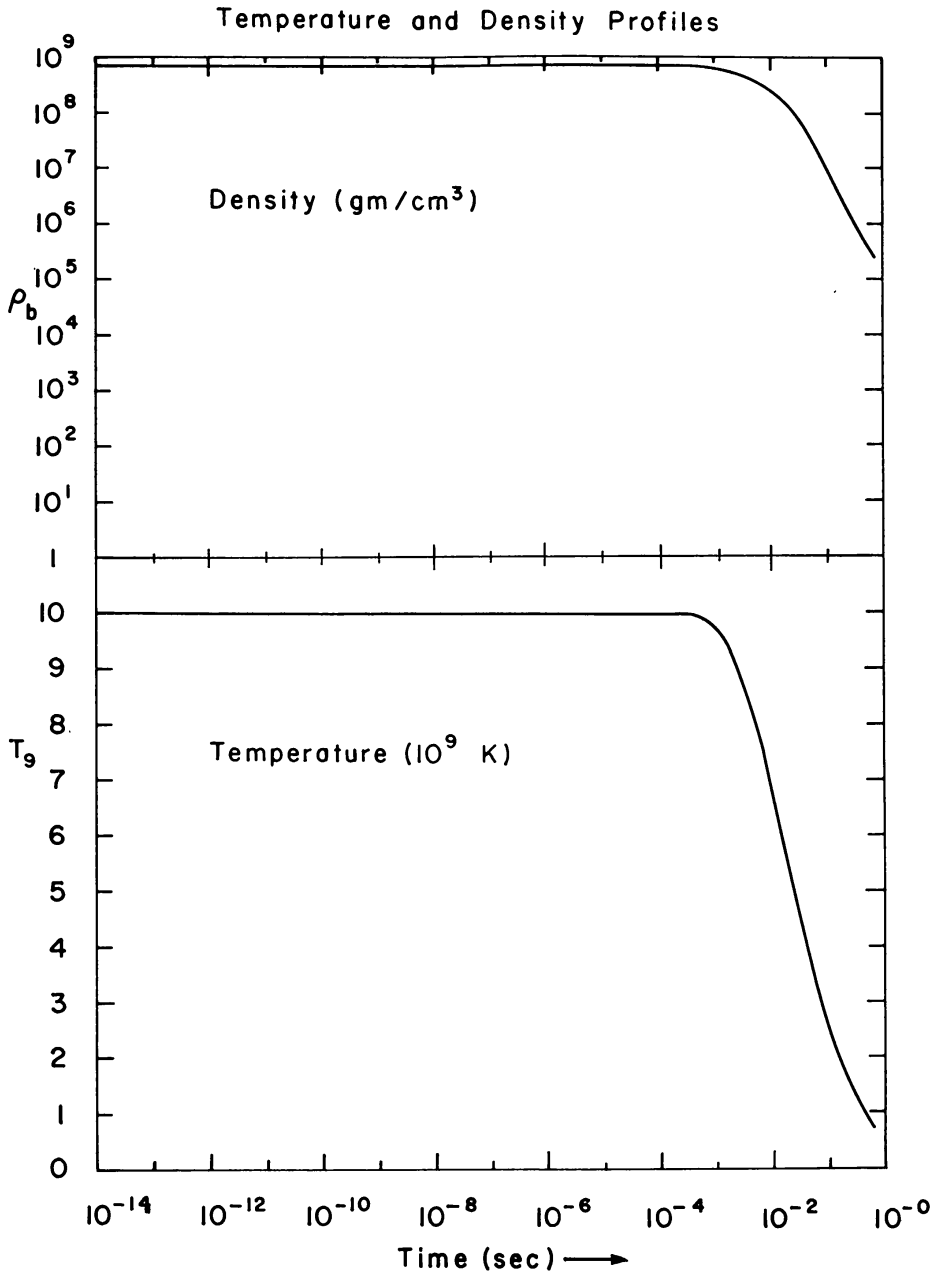

Fig. 1. The temperature and density time evolution used in this calculation.

The different chemical constituents form a *nuclide chart* for the particular problem under consideration and the nuclear reactions, linking one element with another, may be described as reaction *pathways* or *links*. The amalgamation of nuclide chart and reaction links is the *nuclear reaction network*. It is the fundamental tool for nucleosynthesis studies and can run from as few as two nuclei, connected by one reaction, on up to almost unlimited size. In general, its size and applicability are geared to meet the requirements of specific problems. We emphasize its importance,

because an inadequate or inappropriate network will give misleading answers to the questions posed to it.

A. THE NUCLIDE CHART AND THE REACTION RATES

In all, our network contains 903 strong and electromagnetic reactions linking 107 different nuclei. No beta decays were included and the applicability of the network was therefore limited to time scales on the order of beta decay half lives when appreciable amounts of the nuclear material lay off the valley of beta stability. Our calculations, therefore, were always halted before the most β active elements in the network began to decay.

The chart of the nuclei composing the reaction network is shown in Figure 2. Following the $Z=N$ line the nuclei form a rather broad path up through the silicon isotopes. This is the main part of the network and on the average each isotope chain is 5 to 6 nuclei wide with more nuclei on the neutron rich side of the beta stability

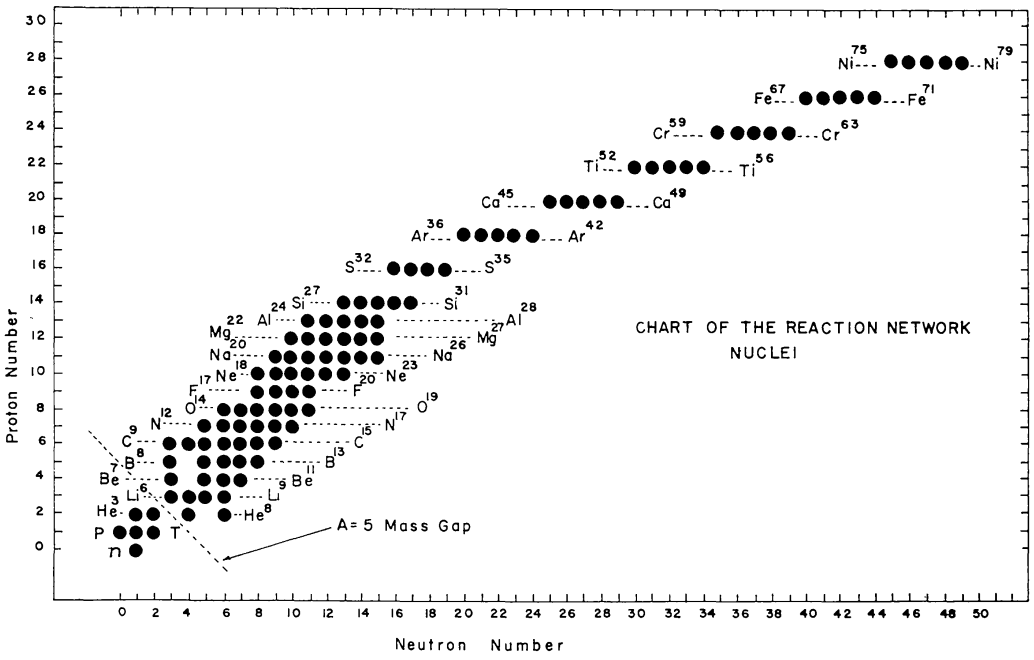

Fig. 2. Nuclide chart of the constituents included in our reaction network. Those above silicon are the extension network nuclei.

line than on the proton rich side. Beyond silicon are the nuclei for the extension network. They are even Z isotopes and veer off the valley of beta stability into the very neutron rich region.

The extension network serves two purposes. First, we were interested, at least qualitatively, in understanding the build up of the heavier elements ($A \geqslant 28$) for neutron rich environments. Therefore, the extension network was directed toward the doubly magic Ni^{78} nucleus, a constituent, which, equilibrium calculations indi-

cated would have a large abundance for our temperature and density freeze out conditions when the neutron to proton ratio was greater than ~ 1.5. Second, the extension network served as a valve or throttle with which to prevent the inevitable pile up distortions in the main part of the network that would have resulted from abruptly ending it at the silicon isotopes.

In order to keep the calculation down to a manageable size, the number of nuclei in the extension network had to be minimized. This results in an underestimate of the speed with which material flows in it, because material is constrained through reaction pathways which are not necessarily the fastest. In this neutron rich region, where there is virtually no reliable experimental data, reaction rates were calculated from theory and the tendency was to overestimate them in order to effect a more realistic flow past silicon.

A detailed account of the handling of all the reaction rates may be found in Delano (1969), but briefly, at least 50% of them were, in one way or another constructed from experimental cross-section measurements in the energy range of interest. Another 25% were pieced together, in a semiempirical manner, from incomplete experimental data, and the remainder had to be estimated theoretically.

B. THE $A=5$ MASS GAP REACTIONS

In any explosive nucleosynthesis problem which starts out with just neutrons and protons, one of the things that inhibits the synthesis of material heavier than He^4 is the mass gap at $A=5$. For this atomic mass number there are no stable or unstable bound nuclei and the flow past helium is normally forced through reactions which by-pass the gap. This is usually done via the triple alpha reaction, the region of constituents lighter than carbon being filled in by endothermic reactions once the carbon has built up.

While there are no bound nuclei at $A=5$ there is a strong resonance ($E_r \sim 0.92$ MeV, $\Gamma \sim 1$ MeV, $J=\frac{3}{2}$) in the neutron-alpha elastic scattering cross-section. Interpreting this as the short lived He^5 nucleus, a formalism was developed which predicts the amounts of an unstable nucleus present in a gas composed of two stable components (Delano, 1970). In a gas of neutrons and alpha particles, at the temperatures and densities which interest us ($T_9 \leqslant 10$, $\varrho \leqslant 10^9$ gm/cm^3), it was found that the fraction of helium in the form of He^5 can go as high as 10^{-4}. In effect then, at sufficiently high densities, the $A=5$ mass gap will be occupied by He^5 which may serve as the target particle in nuclear reactions.

An extensive calculation was undertaken to estimate the rate for the reaction $n+n+He^4 \rightarrow He^6+\gamma$. It turned out to be quite weak, the photodisintegration cross-section for He^6 never rising above a few tenths of a millibarn. By far the most effective reaction proceeding on He^5 was $He^4+n+He^4 \rightarrow Be^9+\gamma$. Part of this proceeds through the branch $Be^8(n, \gamma)Be^9$.

Consideration of other reactions revealed that, besides the triple alpha and its inverse, there are no less than 50 reaction links capable of transporting material back and forth across the $A=5$ mass gap.

$n + n + \mathrm{He}^4 \rightleftarrows \mathrm{He}^6 + \gamma$
$p + n + \mathrm{He}^4 \rightleftarrows \mathrm{Li}^6 + \gamma$
$D + n + \mathrm{He}^4 \rightleftarrows \mathrm{Li}^6 + n$
$D + n + \mathrm{He}^4 \rightleftarrows \mathrm{He}^6 + p$
$D + p + \mathrm{He}^4 \rightleftarrows \mathrm{Li}^6 + p$
$D + n + \mathrm{He}^4 \rightleftarrows \mathrm{Li}^7 + \gamma$
$\mathrm{He}^4 + p + \mathrm{He}^4 \rightleftarrows \mathrm{Be}^7 + D$
$D + \mathrm{He}^4 + \mathrm{He}^4 \rightleftarrows \mathrm{Be}^9 + p$
$T + \mathrm{He}^4 + \mathrm{He}^4 \rightleftarrows \mathrm{Be}^9 + D$
$T + \mathrm{He}^4 + \mathrm{He}^4 \rightleftarrows \mathrm{B}^{10} + n$
$D + \mathrm{He}^4 \rightleftarrows \mathrm{Li}^6 + \gamma$
$T + \mathrm{He}^4 \rightleftarrows \mathrm{Li}^7 + \gamma$
$T + \mathrm{He}^4 \rightleftarrows \mathrm{Li}^6 + n$
$T + n + \mathrm{He}^4 \rightleftarrows \mathrm{Li}^7 + n$
$T + n + \mathrm{He}^4 \rightleftarrows \mathrm{He}^6 + D$
$T + p + \mathrm{He}^4 \rightleftarrows \mathrm{Li}^6 + D$
$\mathrm{He}^4 + n + \mathrm{He}^4 \rightleftarrows \mathrm{Li}^7 + p$
$\mathrm{He}^4 + n + \mathrm{He}^4 \rightleftarrows \mathrm{Be}^9 + \gamma$
$\mathrm{He}^4 + n + \mathrm{He}^4 \rightleftarrows \mathrm{Li}^6 + T$
$\mathrm{He}^3 + \mathrm{He}^4 \rightleftarrows \mathrm{Be}^7 + \gamma$
$\mathrm{He}^3 + \mathrm{He}^4 \rightleftarrows \mathrm{Li}^6 + p$
$\mathrm{He}^4 + \mathrm{He}^4 \rightleftarrows \mathrm{Li}^6 + D$
$\mathrm{He}^4 + \mathrm{He}^4 \rightleftarrows \mathrm{Be}^7 + n$
$\mathrm{He}^4 + \mathrm{He}^4 \rightleftarrows \mathrm{Li}^7 + p$
$\mathrm{He}^4 + \mathrm{He}^4 + \mathrm{He}^4 \rightleftarrows B^{11} + p.$

These are the $A=5$ mass gap reactions in the network and it should be pointed out that many of them have been considered previously by other investigators (most notably Wagoner, 1968). Some of the forward reactions have large energy thresholds so the inverse reaction predominates and material will be transported back across the gap. While this set of reactions virtually eliminates the bottleneck at $A=5$, it must be kept in mind that the three body reactions only become important at high densities and the large number of reactions involving neutrons restricts their applicability to time scales less than 12 min. In short the list is well suited to supernova explosions but does not have wide spread application in other areas of astrophysics.

C. THE NETWORK DIAGRAMS

Graphical representations of the individual reaction links in a network of reactions are potentially quite revealing in the symmetry or lack of it that they display. Unfortunately the present status of these pictures is that different people, discussing the same problem, will draw different graphs. Suited to individual tastes, it is not uncommon to find all the reactions in a network displayed in a single diagram. Completely negating the value of visual presentations, what results is a profusion of interconnecting straight lines, where each line may be mistaken for one of several possible reactions unless it is clearly labeled. In order to remedy this, we have devised a rather natural set of rules for the unambiguous construction of any two body reaction link. When followed, these instructions will permit individual investigators, discussing the same nucleosynthesis problem, to draw separate network diagrams which are visual and topological facsimilies of each other.

(1) The portion of the nuclide chart of interest is laid out on a rectangular grid in the manner of Figure 2. The ordinate denotes neutron number, the abscissa denotes proton number, and each intersection is occupied by an isotope, symbolized by a circle (if the isotope is bound).

(2) In conjunction with the notation $X(a, b)\ Y$ these rules will tell how to connect the circle for the target nucleus, X, to the circle for the residual nucleus, Y, by a

single line which displays the identities of the projectile, a, and the emergent particle, b. An arrow head on the line reveals the direction of the reaction. If the arrow points away from x, x is destroyed; if it points towards x, x is created; and if both the reaction and its inverse are to be included there will be two opposing arrow heads on the same line. We have arbitrarily adopted the convention of placing the arrow head near the nucleus being destroyed.

(3) All reactions involving the emission or absorption of a photon are symbolized by connecting lines with constant curvature. To illustrate for neutrons, neighboring isotopes would be connected by a horizontal straight line pointing to the right for (n, γ) (see Figure 3a) and to the left for (γ, n). Similarly (p, γ) and (γ, p) would have vertical straight lines connecting neighboring isotones, while 45° straight lines would be in order for (D, γ) and (γ, D) reactions. Slightly curved lines, arcs of large circles, would be needed to avoid intersecting nuclei not involved in the reaction in, say (α, γ) or (γ, α) reactions (see Figure 3b).

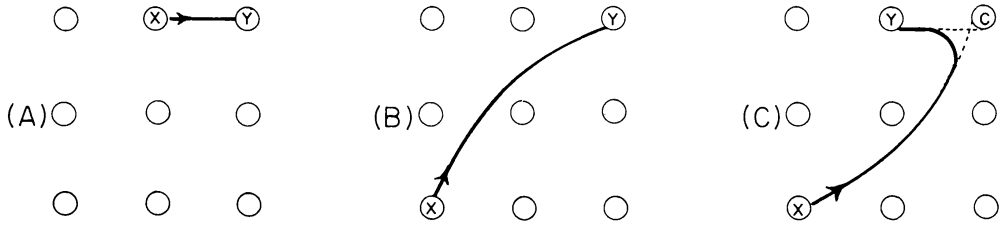

Fig. 3. Illustration for the construction of reaction of reaction links. (A) shows an (n, γ) link; (B) shows an (α, γ) link; and (C) shows an (α, n) link.

(4) To construct particle-particle reaction links of the form $X(a, b)\ Y$ it is necessary to first sketch the two capture lines $X(a, \gamma)$ and $Y(b, \gamma)$. These will intersect at a common nucleus C. Join these two lines by a small curved arc which just misses the circle for nucleus C. The result will be a line joining X and Y with a bend in it. The bend 'points' at C, which may be regarded as the compound nucleus through which the reaction took place. This is illustrated in Figure 3c for the (α, n) reaction.

(5) The curvature of a connecting line linking any two nuclei may go to zero but it must never change sign or intersect itself. This may be accomplished by avoiding the construction of lines with kinks in them. This last rule, with the exception of some trivial cases of left-right symmetry, insures the construction of unique diagrams.

The procedure outlined here, while almost intuitively obvious, in general only applies to two body, and in some cases three body, reactions. It might be elaborated on to include many body and other types of reactions but it is sufficient for our purposes in its present form.

D. THE REACTION LINKS

Figure 4(A) displays the (n, γ), (γ, n), (p, γ) and (γ, p) reaction links. This constitutes the largest single block of reactions with a total of 276 forward and inverse rates.

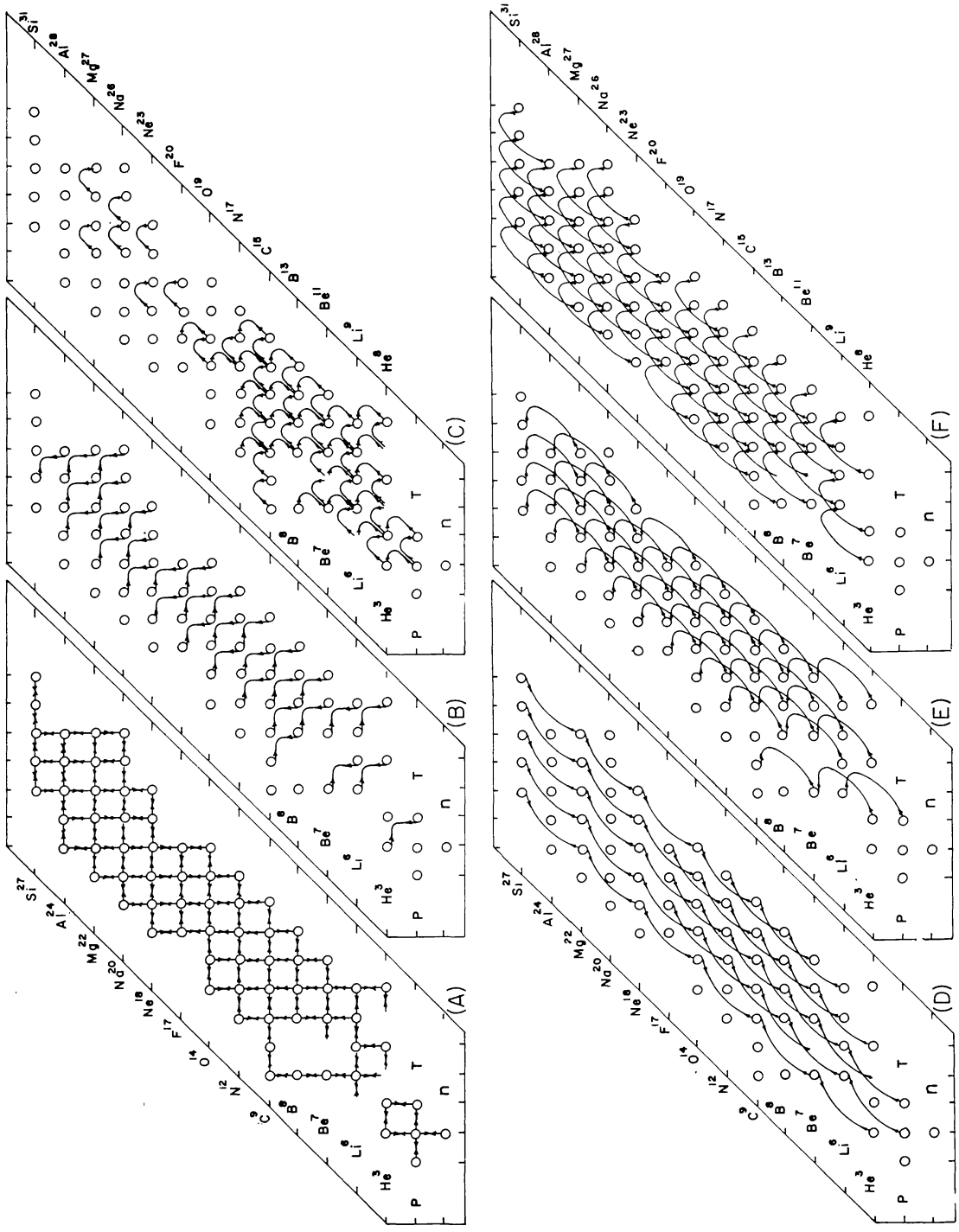

Fig. 4. Diagrams of the nuclear reaction network employed in this calculation. (A) displays the (n, γ), (γ, n) (p, γ) and (γ, p) links; (B) displays the (n, p) and (p, n) links; (C) displays the (D, p), (p, D), (D, n) and (n, D) links; (D) displays the (α, γ) and (γ, α) links; (E) displays the (α, n) and (n, α) links; and (F) displays the (α, p) and (p, α) links.

For each nucleus lighter than sulphur, the 'communication' with the entire network is complete, there being no gaps in the linkage of each individual with its nearest neighbors. Along isotope and isotone lines, these reactions are critical in the approach to and maintenance of nuclear statistical equilibrium. Here and elsewhere, reaction lines will be seen to emerge from or terminate on unoccupied regions of the nuclide chart. These are for reactions involving the unbound nuclei He^5, He^7, Li^5, and Be^8.

The (n, p)–(p, n) reaction links of Figure 4(B) are partially responsible for the local distribution of baryonic material along isobar lines. While not as complete as the (n, γ) and (p, γ) diagram, these reactions, for $A \leqslant 28$, always link together the two most neutron rich nuclei in an isobar.

The inclusion of (D, p), (p, D) and (D, n), (n, D) reactions, shown in Figure 4(C), is a feature not normally found in nucleosynthesis studies. The reason for considering deuteron reactions beyond those leading to the formation of He^4 is two fold. First, in the initial phases in the build up of He^4, deuterium is the third most abundant constituent. And second, since the $A=5$ mass gap reactions are capable of producing material heavier than $A=5$, before helium is completely formed, it was desirable to provide numerous fast pathways for the flow of material between helium and carbon and beyond. In view of this it seemed inappropriate to neglect the large cross-sections generally encountered in stripping and pick up reactions. In this regard there are 94 other reactions involving deuterium, tritium and He^3 not shown in Figure 4. They are (T, n)–(n, T), (T, p)–(p, T), (He^3, n)–(n, He^3), (He^3, p)–(p, He^3), (α, D)–(D, α), (α, T)–(T, α), (α, He^3)–(He^3, α), (T, D)–(D, T), and (He^3, D)–(D, He^3).

The (α, γ)–(γ, α), (α, n)–(n, α) and (α, p)–(p, α) links are shown in Figures 4(D), (E), and (F) respectively. Together they comprise 296 links and are the real 'work-horse' reactions for the transport of material up to silicon.

Beyond silicon is the extension network, shown in Figure 5, where (α, γ) reactions proceed on even Z isotope chains up to nickel. The nuclei of each chain are linked to one another by (n, γ) and (γ, n) reactions.

Not discussed thus far is an assortment of 60–70 reactions which were included on an individual basis. Many were one way destruction reactions of the form $(n, 3n)$ or $(p, 2np)$ while a few were of the 'heavy particle' type e.g. $Li^7 + Li^7 \rightleftarrows He^6 + He^4 + He^4$

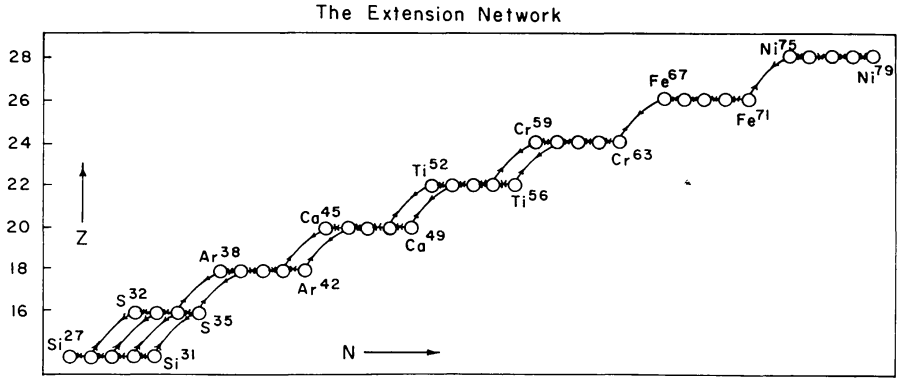

Fig. 5. Display of the (n, γ), (γ, n), (α, γ), and (γ, α) reaction links of the extension network.

or $Li^6 + Li^6 \rightleftarrows B^{10} + D$. They served mainly as tests to see if their presence or non-presence would have any effect on the elements synthesized. For the models studied they were not significant.

It is worth noting that the size and uniformity of this network endow it with properties that can only be described as fluidlike. At times, the distribution of baryonic material in the nuclide chart was reminiscent of the surge wave, seen in the flow of a liquid under a sluice gate. In isolated regions of the network, little eddy currents in the baryonic flow, appeared and disappeared. This has also been the experience of other workers (Truran, 1967).

The continuum features of this network suggest a fluid dynamic approach to the integration of the equations (network equations) governing the rate of change of the abundances of the different nuclei it contains. This has not been done, but the large number of three body nuclear reactions involved introduces additional complications for some of the more standard finite difference techniques. The modifications needed in the numerical integration of the network equations are discussed in the appendix.

4. Supernova Nucleosynthesis

The graphs of Figures 6–9 display the time evolution of the abundances for the three different initial neutron to proton ratios. In these plots the 'abundance' is actually the mass fraction of a constituent divided by its mass number. The most striking property of these curves is the speed with which the system establishes nuclear statistical equilibrium (approximately horizontal straight lines for the abundances). In less than a billionth of a second all the isotopes lighter than silicon have come into equilibrium with each other. This remained a general feature of all the models studied.

It is no accident that the slow down always occurred at the point where the extension network begins. This is a vivid demonstration of the inadequacies of bare network chains in the study of nucleosynthesis, under conditions of high temperature and density. The skeleton chain, while fast enough to 'drain off' any discernable 'pile up' distortions among the light nuclei, underestimates the speed with which baryons flow to the heavy end of the network by several orders of magnitude. By a simple, but rough, empirical extrapolation of the present results, it is possible to estimate that a realistic network chain beyond silicon would speed up the flow of nuclear material to the point where the heaviest constituent in the network, Ni^{79}, would come into equilibrium with the system in time scales not greater than 10^{-8} sec. This is for a temperature and density of 10^{10} K and 7×10^8 gm/cm^3. With the present extension network it takes between 10^{-5} and 10^{-4} sec for rough equilibrium to obtain. After the 10^{-8} sec (or 10^{-5}–10^{-4} sec for the present network), needed to establish equilibrium, the system stays in equilibrium (approximately horizontal straight lines) until the temperature and density start decreasing at 10^{-3} sec. At this point the abundances begin to readjust, changing to maintain equilibrium with the new temperature and density values at each point in time. This continues until the charged particle reactions begin to freeze out at 10^{-2} sec.

A. THE LIGHT NUCLEI

Figure 6 shows the abundance plots of the so called 'X process' elements D, Li, Be, and B (Aller, 1961) for the $N/P=4$ case. As the temperature and density begin to decrease in the expanding gas, the abundances of these elements begin to assume values consistent with those measured in the solar system and it was hoped that they might survive the explosion. They do not. For the two cases $N/P=\frac{3}{2}$ and $N/P\sim 1$ (not shown), they are almost completely consumed in the production of heavier material by the time (10^{-2} sec) the gas has cooled to the point where the time scales

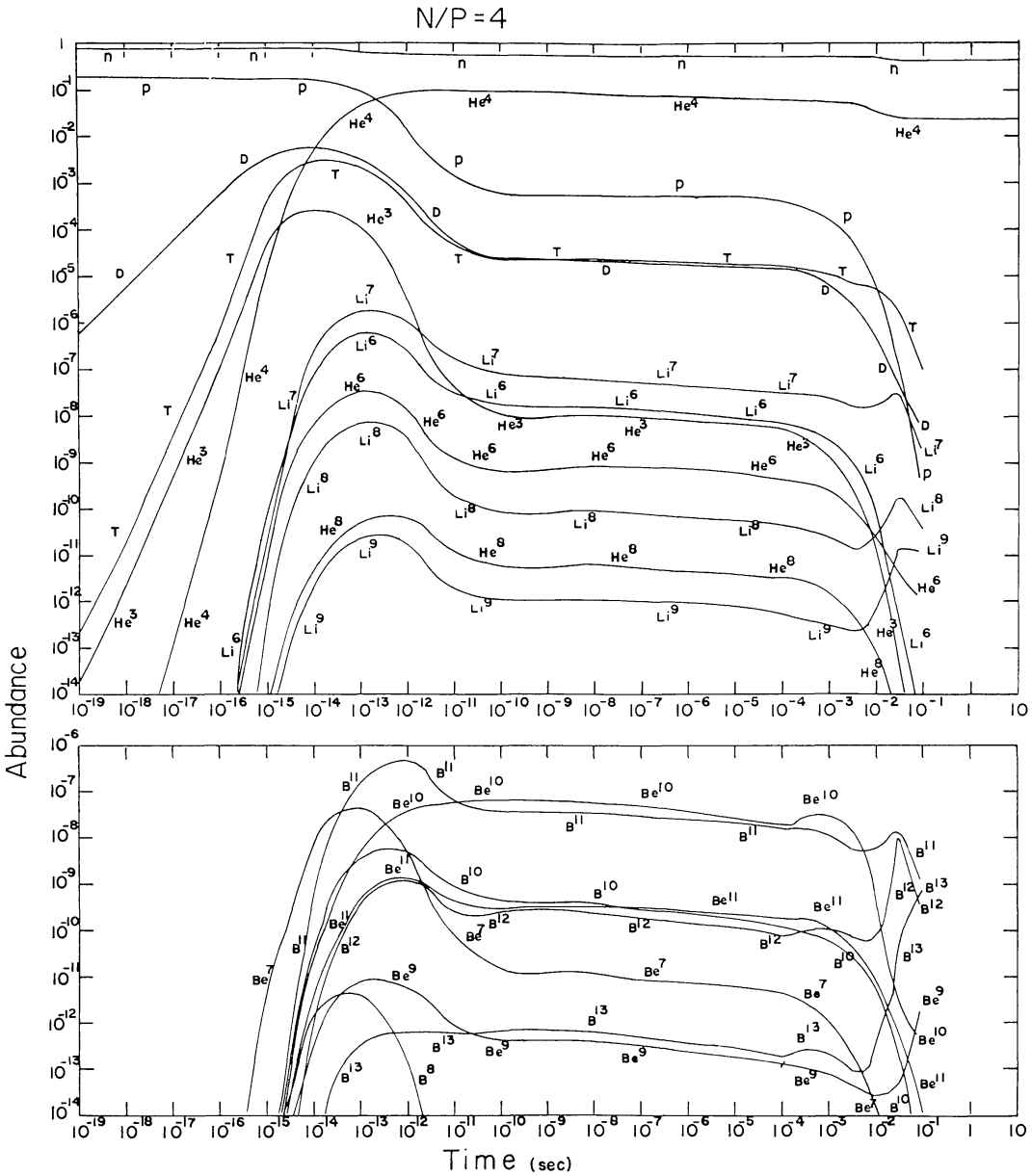

Fig. 6. Formation and destruction of the X-process elements. Horizontal portions indicate local statistical equilibrium.

for charged particle reactions exceed the hydrodynamic expansion time scale. During freeze out, however, the abundances of these elements did mimick, temporarily, their solar system values. In the $N/P=4$ model, those that linger after the charged particle freeze out, will be obliterated by the rapid capture of neutrons.

While indicating the inhospitality of supernova explosions to D, Li, Be, and B the results do suggest that explosive conditions might provide an alternative to the spallation reactions thought to be responsible for the synthesis of these elusive elements. Since, only a narrow range of initial temperatures and densities were considered in this work, nothing really compelling can be said about the optimum explosive conditions for synthesizing the X-process elements. It may nevertheless be worthwhile to state those gleaned, even from the restricted choice of initial conditions studied here.

Initial n to p Ratio	$1 \leqslant n/p \leqslant \frac{3}{2}$
Initial Temperature	$T \sim 10^{10}$ K
Initial Density	$\varrho \sim 7 \times 10^{8}$ gm/cm^3
Hydrodynamic Freeze Out Time Scales	10^{-8} sec $\leqslant \tau_f \leqslant 10^{-5}$ sec.

This is not very different from the profiles of Wagoner (1968, 1969), who was investigating light element synthesis in galactic core explosions and elsewhere (but not supernovae). While promising, it must be noted that these conditions probably imply highly relativistic expansion velocities and correspond to no observed stellar or cosmic event.

B. CARBON AND BEYOND

Figures 7, 8, and 9 display representative plots for the respective neutron to proton ratios: $n/p=4$, $n/p=\frac{3}{2}$ and $n/p \sim 1$. In each figure, if an isotope chain is represented by a plot of one of its members, it is the most abundant constituent in the chain that is shown. These graphs are best interpreted by referring to the nuclide chart and extension network of Figures 2 and 5. These abundance plots have features which reflect both the choice of initial conditions and the distortions introduced by the limited size of even this sizeable network. It is necessary to distinguish between them in order to make meaningful statements about some of the conditions under which the r-process may take place in supernova explosions.

One obvious feature which reflects the choice of initial conditions is the weight of the n to p ratio in determining where the products of nucleosynthesis will lie. For $n/p=4$, the most neutron rich isotopes in each isotope chain tend to be the most abundant, while for $n/p \sim 1$, material tends towards the $Z=N$ line. In the $n/p=\frac{3}{2}$ case, for which the network is probably best suited, virtually all of the baryonic mass is distributed among those nuclei which lie in the center of the extension network.

The most serious distortions introduced by the incompleteness of the network are those due to the extension network. The smaller number of reaction links in this region, distorts the flow time of baryons in it. This is most critical at freeze out when the system is losing communication with itself, through its charged particle

reactions, and is falling out of equilibrium. Perhaps even more severe, is the fact that material flowing up past silicon, is constrained to the extension network; a region it might not ordinarily choose. In evidence of this, is the high abundances of the α particle nuclei in the $n/p \sim 1$ plots of Figure 9. It is clear, that in a broader extension network, Ar^{36} and Ca^{40} would have been favored over Ar^{38} and Ca^{45}. In all probability a realistic network for this n to p ratio would have produced an abundance distribution resembling the iron peak, with Fe^{56} the most favored. As a possible candidate for describing the r-process, however, this model must be rejected since all the neutrons are depleted by the time the necessary seed nuclei are produced.

In spite of the limitations enumerated above, certain definite conclusions may be drawn from our results. The expansion time scales in these supernova models are long enough, under the stated conditions of temperature and density, to allow the synthesis of significant amounts of material, at least as heavy as iron or nickel. There can be no doubt that these models are capable of producing the seed nuclei needed for r-process. The remaining question is, which ones are the most abundant and what amounts of neutrons will they be exposed to?

On this point, we must, of necessity, be somewhat vague. Our results, however, are capable of suggesting a rough rule of thumb in constructing starting conditions for the r-process. The final distribution of the elements after freeze out, tend to reflect the temperature and density at freeze out; ($2 \leqslant T_9 \leqslant 4$ and $\varrho_b \sim 10^6$–10^8 gm/cm^3 for

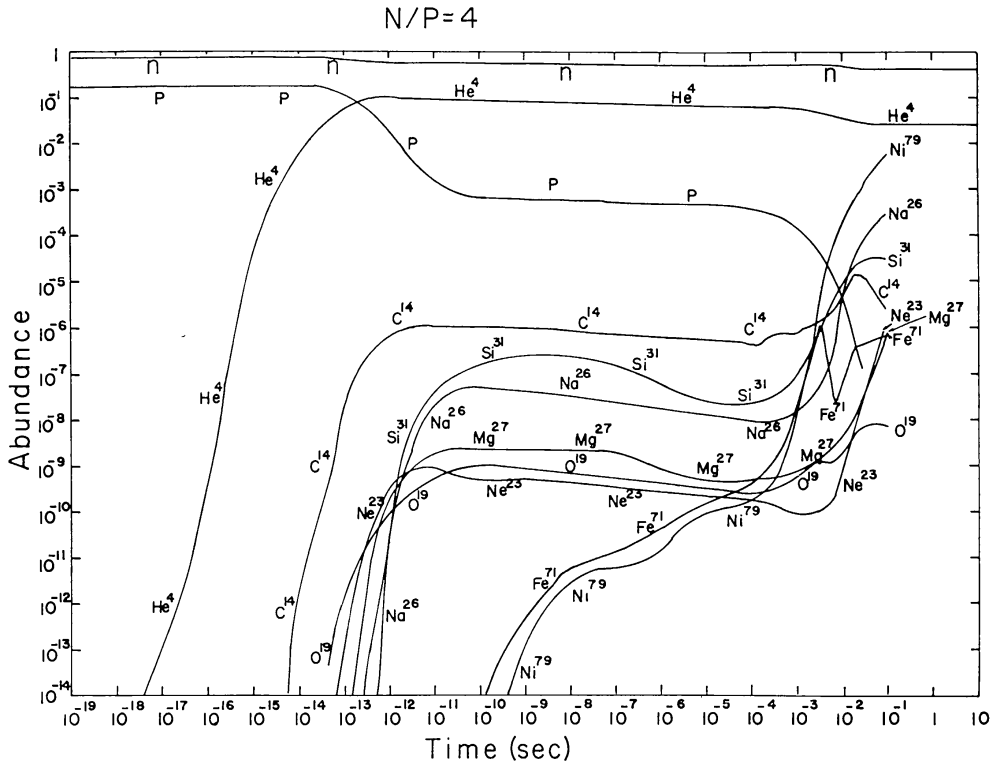

Fig. 7. Synthesis products for the $N/P = 4$ ratio. An isotope chain is represented by its most abundant constituent.

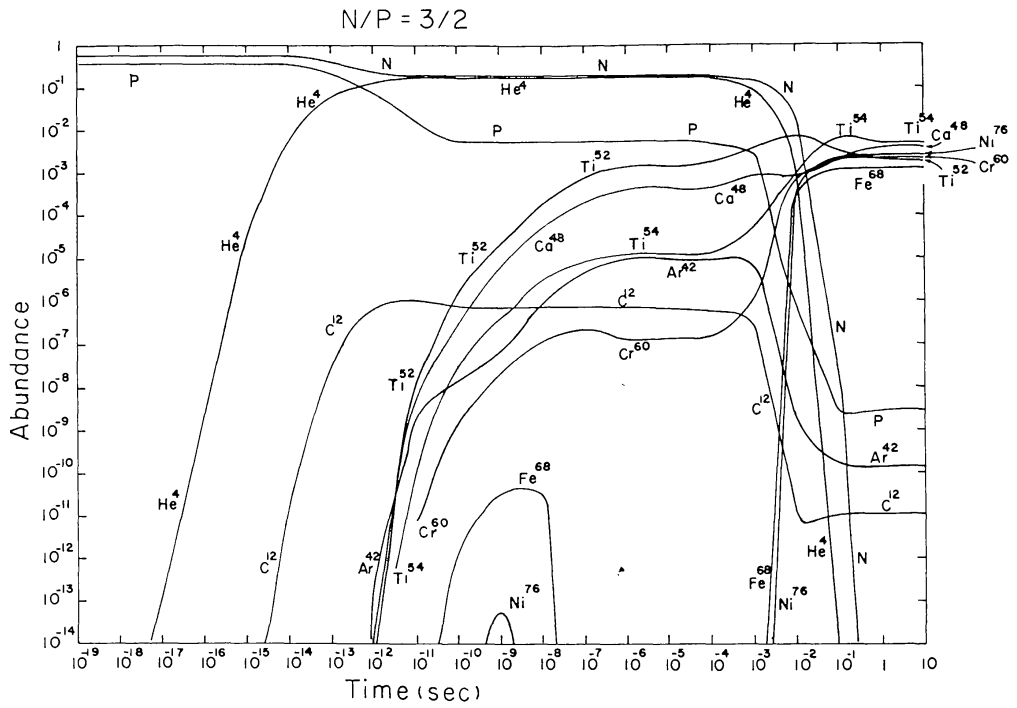

Fig. 8. Synthesis products for the $N/P = \frac{3}{2}$ ratio. An isotope chain is represented by its most abundant constituent.

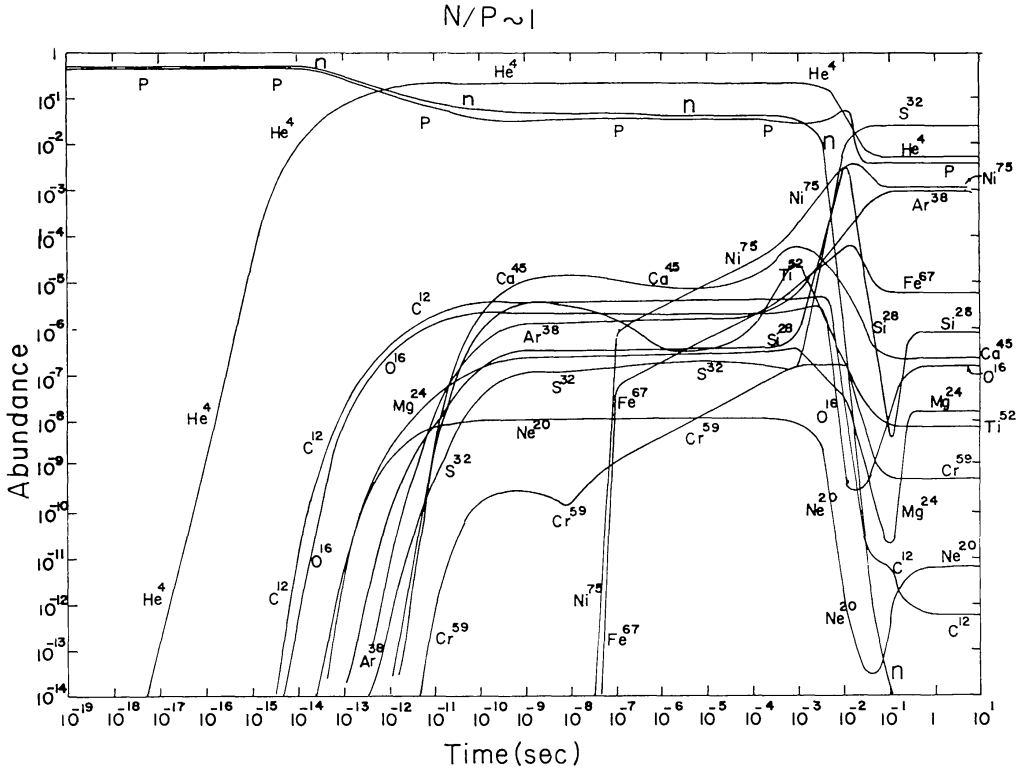

Fig. 9. Synthesis products for the $N/P \sim 1$ ratio (51% neutrons and 49% protons). An isotope chain is represented by its most abundant constituent.

the present model). That is, the assumption, that nuclear reactions are fast enough to establish a condition of nuclear statistical equilibrium among the different constituents, at the time of freeze out, is a reasonable approximation to the actual situation. This has been discussed in detail by Truran *et al.* (1968); the equations of nuclear statistical equilibrium (Hoyle, 1946) may be used to determine the number density of any constituent, in terms of the free neutron and proton number densities and the temperature and mass density of the gas.

It is important to recognize that, as starting conditions, the freeze out temperatures and densities would not produce these equilibrium abundances from just neutrons and protons, in times equal to or less than the hydrodynamic expansion time scales (10^{-3}–10^{-2} sec). This equilibrium, can only be established, within the allotted time, by making adjustments on the synthesis products of higher temperatures and densities.

With the initial conditions $T=10^{10}$ K and $\varrho=7\times10^{8}$ gm/cm^3, it will be seen from Figures 7–9, that of the three n to p ratios considered, only $n/p=4$ does not deplete the neutrons. The implications of this are that, at the *weak interaction* freeze-out, the n to p ratio must be greater than $\frac{3}{2}$ in order that the supernova be a candidate for the r-process. Somewhat lower initial densities would favor a less neutron rich environment for the seed nuclei. In view of the observed supernova rate of 1 per century per galaxy and assuming a mass ejection of $1\,M_\odot$ for each supernova, it is clear, for the three cases studied, that only a small fraction (10^{-4}–10^{5}) of the actual supernova processed mass in our galaxy, has experienced the conditions presented in this paper. The large amounts of heavy elements, produced under these conditions, would contradict the measured solar system abundances, otherwise (Truran *et al.*, 1968).

C. THE ONSET OF THE *r*-PROCESS

As is often the case in scientific endeavor, areas of concentrated effort tend to become disjointed topics in what is, in fact, a continuing sequence of events. Practical considerations often make this unavoidable. It is therefore gratifying to be able to exhibit, explicitly, the smooth transition from the production of the r-process seed nuclei to the onset of the r-process itself. This is, of course, not proof that the r-process actually takes place in this manner; it merely illustrates the compatibility of the supernova models, outlined in Section 2, and some of the suggested physical conditions for producing the heavy elements.

Focussing attention on the nickel isotope chain, for the $n/p=4$ model, in the last moments of the calculation, examination of Figure 10 will reveal the transition to the r-process. In these abundance plots, each open circle represents one of the five isotopes in the chain. The solid lines connecting them, are only intended as a 'guide to the eye'.

Treated like a segment of motion picture film, the first frame is at 1.18×10^{-2} sec after the start of the calculation, when the temperature has decreased to about 6.5 billion degrees from an initial value of 10 billion. Charged particle reactions are still in operation here, with the (α, γ) reactions of the extension network, providing the baryonic flow paths up to the Ni chain. In the third frame, at 2.30×10^{-2} sec,

the temperature is down to around 5 billion degrees and the charged particle reactions are just starting to freeze out. At 3.23×10^{-2} sec, in the fourth frame, the temperature is 4 billion degrees and freeze out is in operation. Communication with the rest of the network has been severed. Alpha particle reactions no longer shuffle nuclear material back and forth between the Ni chain and the Fe chain below it.

It will be noted that at these freezing conditions, $T_9 = 4$ and $\varrho = 6.5 \times 10^7$ gm/cm^3, the most abundant nucleus by mass, with the exception of the neutron, is the doubly magic Ni^{78} nucleus. With reference to the statistical equilibrium calculations of Truran *et al.* (1968) this tends to confirm the statement made earlier, that a reasonable approximation to the freeze out element abundances are those predicted by the equations of nuclear statistical equilibrium under the freeze out conditions.

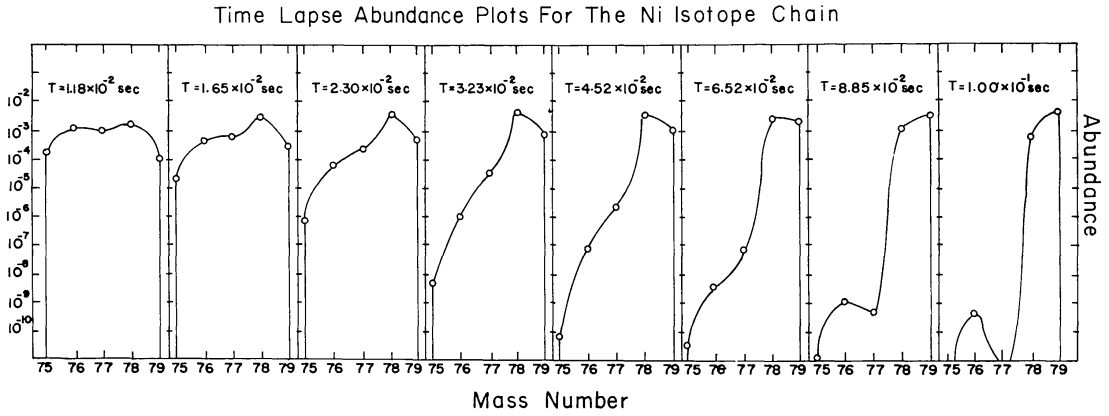

Fig. 10. Sequence of abundance plots exhibiting the onset of the *r*-process in the $N/P = 4$ model.

Isolated, the nuclei of the Ni isotope chain must now come into equilibrium with each other and the large sea of neutrons, by (n, γ) and (γ, n) reactions. In going from the fourth to the eighth frame (10^{-1} sec) the temperature decreases to 2.5 billion degrees. The diminishing temperature is accompanied by a decrease in the rate of photo-neutron reactions, so that by 10^{-1} sec, the least neutron rich part of the chain is consumed, by neutron captures, in building up the most neutron rich. Now, Ni^{79} is the most abundant nucleus.

In this time period (3.23×10^{-2} sec–10^{-1} sec), had the network continued past nickel to copper and zinc and beyond, and had β decays been included, we would have, in point of fact, been witnessing the initial phases of the *r*-process. The zinc isotopes, resulting from the nickel isotope β decays, would have been swept far from the valley of β stability by the rapid capture of neutrons from the surrounding neutron sea. Beta decaying into copper, the process would have continued on upward until either the neutron sea was depleted or the density decreased to the point where neutron capture reactions were negligible. Then the lingering, neutron rich members of each isotope chain would have β decayed to the valley of β stability, leaving, one hopes, the *r*-process elements.

5. *r*-Process Starting Conditions

At freeze out, the conditions for the *r*-process resemble, some what, those prescribed by Seeger *et al.* (1965). There are roughly 65 neutrons per seed nucleus (Ni^{78}), which is sufficient to produce the abundance peak at $A=130$. The temperature is 4 billion degrees and the exposure time to neutrons will be on the order of a second. Where our results, and those of Truran *et al.* (1968), significantly depart from the prescriptions of Seeger, is in the mass density of the expanding gas. Seeger gives, 10^4 gm/cm^3, where as, our results indicate that the *r*-process will start at $\varrho = 6.5 \times 10^7$ gm/cm^3.

The three to four orders of magnitude discrepancy in the density are due in large part to the physical conditions prior to the onset of the *r*-process. Assuming that the initial seed nuclei are the iron peak elements, Seeger *et al.* (1965), have been able to estimate, that, in order to produce the two abundance peaks at $A=80$ and 130, a neutron exposure time of $\Delta t \sim 4$ sec is needed when the temperature is $T_9=2.43$. Equating the free fall time, $\Delta t=(24\pi G\varrho)^{-1/2}$, with the explosion time scale, the 4 sec exposure time is used to arrive at the 10^4 gm/cm^3. All this is based on pre *r*-process starting conditions of α particles and neutrons, resulting from the iron to helium conversion ($Fe^{56} \rightarrow 13\alpha + 4n$), after the collapse of $10^5 M_\odot$ object (Hoyle and Fowler, 1960). Waiting for the alpha particles to 'leak' to C^{12}, via the slow triple alpha reaction, it becomes necessary for the charged particle reactions to freeze out, leaving Fe^{56}, α particles, and enough neutrons (75 per Fe^{56} nucleus) to get to the $A=130$ abundance peak.

In the high density neutron rich environment, in the present model, there is no bottle neck at the $A=5$ mass gap, due to the many three body reactions bridging it. In fact, the triple α reaction could be taken out of the network altogether, with no significant alteration of the final results. Material would flow past $A=5$, mainly by $He^4 + He^4 + n \rightarrow Be^9 + \alpha$, a reaction which was not considered by Hoyle and Fowler (1960) and Seeger *et al.* (1965). By the time the *r*-process begins, we are already at the $A=80$ mass peak, with enough neutrons to take us to the one at $A=130$.

Criticisms of early supernova models, at this late date, are of course redundant and unwarranted. In view of the large scale uncertainties associated with the handling of neutrino energy transport, it is certain, that the models advocated here await refinement and perhaps replacement. It may even be, that most supernovae explode by nuclear detonations, with none of the ejected matter ever reaching the high density, neutron rich phase (Arnett, 1969). But, abstracting nucleosynthesis from specific stellar models, it is necessary to bring into serious question the mechanism envisioned by Hoyle and Fowler (1960) and Seeger *et al.* (1965), whereby we are led to *r*-process starting conditions of Fe^{56} seed nuclei exposed to large numbers of neutrons.* Starting with just neutrons and alpha particles, in the ratio $X_\alpha/X_n=13$,

* We, of course, do not exclude Fe^{56} and neutrons as a possible starting condition for the *r*-process. Our criticism is directed at the suggested sequence of events leading to this environment.

their total reliance on the very slow triple alpha reaction, to bridge the $A=5$ mass gap, guarantees the synthesis of very little Fe^{56}, and hence a large number of neutrons per Fe^{56} nucleus, at the time of the charged particle freeze out. Under the same conditions, the reaction $He^4+He^4+n\rightarrow Be^9+\gamma$, would completely negate the effects of this mechanism. Comparing the rate of alpha particle consumption for the two reactions, we find from Wagoner (1969), at 2 billion degrees, $R_{3\alpha}/R_{2\alpha n}\simeq 3.6\times 10^{-5}\ X_\alpha/X_n$, and from Delano (1969), at 8 billion degrees, $R_{3\alpha}/R_{2\alpha n}\simeq 2\times 10^{-3}\ X_\alpha/X_n$. In effect then, with alpha particles and neutrons being consumed 2 to 4 orders of magnitude faster than supposed by Hoyle *et al.*, there will not be enough neutrons around for the *r*-process when the charged particles freeze out.

One could conceivably circumvent the difficulty of these fast three body reaction rates in the models proposed by Hoyle and Fowler by postulating lower temperatures and densities. But this would then probably work against the high temperature collapse conditions, needed for the initial photodisintegration of Fe^{56} into neutrons and alpha particles. The plausibility of this model must therefore remain in doubt.

6. Conclusion

With a complete network of reactions, up through the silicon isotopes, we have found the products of charged particle nucleosynthesis, in the supernova models studied, to be, in general, heavier than $A=28$. This establishes the compatibility of the freeze out time scales (10^{-2} sec), for these models, and the production of seed nuclei for use in the *r*-process later on in the explosion. Even in the bare extension network beyond silicon, where the time scales for baryonic flow must be regarded as lower limits, our results suggest that at freeze out, the equations of nuclear statistical equilibrium will give reasonable predictions for the element abundances present. This is important, because it allows one the confidence to select *r*-process starting conditions, in these models, by performing a statistical equilibrium calculation at the freeze out temperature and density instead of performing the more time consuming nucleosynthesis calculation.

Having demonstrated, at least qualitatively, that the *r*-process had actually begun, at the termination of one of the calculations, it would appear that the supernova models presented here are plausible candidates for the *r*-process. Along with J. Truran, the authors are now engaged in a full-fledged calculation of the *r*-process, using the starting conditions suggested by this work.

Appendix

NUMERICAL INTERGRATION OF THE NETWORK EQUATIONS

In a gas of nuclei, where nuclear reactions are transmuting the relative amounts of the different species, the rate of change of the number density of a particular constituent can be written as the sum of one-body, two-body, three-body, etc., reaction terms.

$$\frac{dn_i}{dt} = \underbrace{\sum_j \lambda_j^{(i)} n_j}_{\text{1-body}} + \underbrace{\sum_{j \geq k} n_j n_k \langle \sigma_{jk} v_{jk} \rangle^{(i)}}_{\text{2-body}} + \cdots . \tag{A1}$$

The sign of each individual term in a sum is either plus or minus according to whether the i_{+h} constituent is created or destroyed by the reaction that the term represents. The superscript (i) indicates that it is the i_{+h} constituent which is created or destroyed by the reaction.

Instead of number densities we have found it convenient to work with a quantity which we call abundance. It is defined by

$$X_i \equiv \frac{n_i}{\varrho_b N_a}, \tag{A2}$$

where ϱ_b is the mass density in the gas and N_a is Avogadro's number. The abundance of the i_{+h} constituent multiplied by its mass number will give its mass fraction; i.e. the fraction of the total nuclear mass in the form of the i_{+h} constituent. For nuclear reactions among n different constituents the condition of baryon conservation is therefore

$$\sum_{i=1}^{n} A_i X_i = 1 , \tag{A3}$$

where A_i is the mass number of the i_{+h} constituent.

Using Equations (A1) and (A2) and only considering one, two and three body nuclear reactions the differential equations governing the time evolution of the n different species are of the form

$$\left.\begin{aligned}
\frac{dX_1}{dt} &= \sum_j \lambda_j^{(1)} X_j + \sum_{j \geq k} [j, k]^{(1)} X_j X_k + \sum_{j \geq k \geq l} [j, k, l]^{(1)} X_j X_k X_l , \\
&\vdots \qquad\qquad \vdots \qquad\qquad\qquad \vdots \\
\frac{dX_i}{dt} &= \sum_j \lambda_j^{(i)} X_j + \sum_{j \geq k} [j, k]^{(i)} X_j X_k + \sum_{j \geq k \geq l} [j, k, l]^{(i)} X_j X_k X_l , \\
&\vdots \qquad\qquad \vdots \qquad\qquad\qquad \vdots \\
\frac{dX_n}{dt} &= \sum_j \lambda_j^{(n)} X_j + \sum_{j \geq k} [j, k]^{(n)} X_j X_k + \sum_{j \geq k \geq l} [j, k, l]^{(n)} X_j X_k X_l .
\end{aligned}\right\} \tag{A4}$$

These constitute a set of n, coupled, first order, nonlinear differential equations and are sometimes referred to as the 'network equations'. It should be understood that the rate coefficients λ_j, $[j, k]$, and $[j, k, l]$ are in general functions of the gas temperature and density, which may be changing with time. In what follows it shall always be assumed that these coefficients are slowly varying and are approximately constant over some small time interval.

We shall present two numerical techniques for integrating the network equations. The first, kindly furnished to us by Dr. James Truran, is probably a widely used one

in explosive nucleosynthesis problems, but seems to have had very little description in the literature. The second method is essentially a modified version of the first.

FIRST ORDER BACKWARD DIFFERENCING AND MATRIX INVERSION

The backward differencing scheme assumes that the change in X_i in going from the m_{+h} to the $m+1$ time period is given by the value of all X_j at the $m+1$ time period. According to this prescription, Equation (A4) for X_i may be approximated by

$$\frac{X_i^{m+1}-X^m}{t_{m+1}-t_m}=\sum_j \lambda_j^{(i)}X_j^{m+1}+\sum_{j\geqslant k}[j,k]^{(i)}X_j^{m+1}X_k^{m+1}+\sum_{j\geqslant k\geqslant l}[j,k,l]^{(i)}X_j^{m+1}X_k^{m+1}X_l^{m+1}.$$

Defining $\Delta X_i=X_i^{m+1}-X_i^m$ as the change in X_i over the two time periods and $\Delta t=t_{m+1}-t_m$ as the time step or increment this may be written as

$$\frac{\Delta X_i}{\Delta t}=\sum_j \lambda_j^{(i)}(X_j^m+\Delta X_j)+\sum_{j\geqslant k}[j,k]^{(i)}(X_j^m+\Delta X_j)(X_k^m+\Delta X_k)+\sum_{j\geqslant k\geqslant l}[j,k,l]^{(i)}(X_j^m+\Delta X_j)(X_k^m+\Delta X_k)(X_l^m+\Delta X_l). \tag{A5}$$

Performing the indicated multiplications and neglecting terms higher than first order in the ΔX_j results in, after some algebraic manipulation,

$$-\frac{\mathrm{d}X_i}{\mathrm{d}t}=\Delta X_1M_{i1}+\Delta X_2M_{i2}+\cdots+\Delta X_iM_{ii}+\cdots+\Delta X_nM_{in}, \tag{A6}$$

where $\mathrm{d}X_i/\mathrm{d}t$ is given by Equation (A4) and

$$M_{ij}=-\frac{\delta_{ij}}{\Delta t}+\lambda_j^{(i)}+\sum_k[j,k]^{(i)}X_k^m+\sum_{k\geqslant l}[j,k,l]^{(i)}X_k^mX_l^m. \tag{A7}$$

In effect then, the n coupled differential equations of (A4) have been reduced to a linear system of n simultaneous algebraic equations for the ΔX_j:

$$\left.\begin{aligned}
-\frac{\mathrm{d}X_1}{\mathrm{d}t}&=\Delta X_1M_{11}+\Delta X_2M_{12}+\cdots+\Delta X_jM_{1j}+\cdots+\Delta X_nM_{1n},\\
-\frac{\mathrm{d}X_2}{\mathrm{d}t}&=\Delta X_1M_{21}+\Delta X_2M_{22}+\cdots+\Delta X_jM_{2j}+\cdots+\Delta X_nM_{2n},\\
&\vdots\\
-\frac{\mathrm{d}X_j}{\mathrm{d}t}&=\Delta X_1M_{j1}+\Delta X_2M_{j2}+\cdots+\Delta X_jM_{jj}+\cdots+\Delta X_nM_{jn},\\
&\vdots\\
-\frac{\mathrm{d}X_n}{\mathrm{d}t}&=\Delta X_1M_{n1}+\Delta X_2M_{n2}+\cdots+\Delta X_jM_{nj}+\cdots+\Delta X_nM_{nn}.
\end{aligned}\right\} \tag{A8}$$

After computing the $\mathrm{d}X_i/\mathrm{d}t$ and M_{ij} terms, the n ΔX_i may be solved for by the method of determinants, more commonly called matrix inversion. The abundances

and the time step can then be updated, $X_i^{m+1} = X_i^m + \Delta X_i$, $t_{m+1} = t_m + \Delta t$, and the entire process repeated.

This procedure is extremely fast and typically allows a 1% increase in the size of the time step, Δt, over the previous time step. It is, however, incapable of handling a network containing any reasonable selection of three body nuclear reactions where all three bodies are nonidentical. In Equation (A5) two body reaction terms are proportional to $(X_j+\Delta X_j)\,(X_k+\Delta X_k)$ while three body terms have $(X_j+\Delta X_j)\,(X_k+\Delta X_k)\,(X_l+\Delta X_l)$. Carrying out the multiplications and saving terms to all orders in the ΔX_i we will have terms of the form

	0_{+h} Order	1st Order	2nd Order	3rd Order
2-Body Reactions	X_jX_k	$X_j\Delta X_k$ $X_k\Delta X_j$	$\Delta X_j\Delta X_k$	
3-Body Reactions	$X_jX_kX_l$	$X_jX_k\Delta X_l$ $X_jX_l\Delta X_k$ $X_kX_l\Delta X_j$	$X_j\Delta X_k\Delta X_l$ $X_k\Delta X_j\Delta X_l$ $X_l\Delta X_j\Delta X_k$	$\Delta X_j\Delta X_k\Delta X_l$

If $\Delta X_j < X_j$, $\Delta X_k < X_k$, and $\Delta X_l < X_l$ it is clear for the two body reactions that second order terms will be less than first order terms. For three body reactions this is not always the case. If for example, $\Delta X_l \sim 0$ but $\Delta X_j \neq 0$ and $\Delta X_k \neq 0$ it is evident that $|X_l\Delta X_j\Delta X_k| > |X_jX_k\Delta X_l|$. Consequently the approximation that neglected terms higher than first order in the ΔX_i is in general not valid for three body nuclear reactions. Because our network contains many of these reactions we found it necessary to modify somewhat this differencing technique.

THE LINEARIZED ERROR APPROXIMATION FOR BACKWARD DIFFERENCING

Equation (A5) related the changes in the X_i when using the backward differencing method.

$$0 = -\frac{\Delta X_i}{\Delta t} + \sum_j \lambda_j^{(i)} (X_j + \Delta X_j) + \sum_{j \geq k} [j, k]^{(i)} (X_j + \Delta X_j)(X_k + \Delta X_k) + \sum_{j \geq k \geq l} [j, k, l]^{(i)} (X_j + \Delta X_j)(X_k + \Delta X_k)(X_l + \Delta X_l). \quad \text{(A5)}$$

The time period superscripts (m) have been dropped for convenience. Suppose we have initial guesses for the ΔX_i, call them $\Delta Y_i^{(0)}$. Then $\Delta X_i = \Delta Y_i^{(0)} + \varepsilon_i^{(0)}$, where $\varepsilon_i^{(0)}$ is the error in this guess, and (A5) may be rewritten.

$$\begin{aligned} f_i(\Delta Y_1^{(0)} + \varepsilon_1^{(0)}, \Delta Y_2^{(0)} + \varepsilon_2^{(0)}, \ldots, \Delta Y_i^{(0)} + \varepsilon_i^{(0)}, \ldots, \Delta Y_n^{(0)} + \varepsilon_n^{(0)}) &= 0 \\ = -\frac{(\Delta Y_i^{(0)} + \varepsilon_i^{(0)})}{\Delta t} &+ \sum_j \lambda_j^{(i)} (X_j + \Delta Y_j^{(0)} + \varepsilon_j^{(0)}) \\ + \sum_{j \geq k} [j, k]^{(i)} (X_j + \Delta Y_j^{(0)} + \varepsilon_j^{(0)})(X_k + \Delta Y_k^{(0)} + \varepsilon_k^{(0)}) &+ \sum_{j \geq k \geq l} [j, k, l]^{(i)} (X_j + \Delta Y_j^{(0)} + \varepsilon_j^{(0)}) \\ \times (X_k + \Delta Y_k^{(0)} + \varepsilon_k^{(0)})(X_l + \Delta Y_l^{(0)} + \varepsilon_l^{(0)}). \quad \text{(A9)} \end{aligned}$$

If the initial guesses are close to the actual values, the errors, ε_i, will be small and each $f_i(\Delta Yj+\varepsilon_1, \ldots, \Delta Y_i+\varepsilon_i, \ldots)$ may be expanded in a Taylor series, about the ΔY_i, which is linear in these errors. That is, only terms to first order in ε_i are saved.

$$f_i(\Delta Y_1 + \varepsilon_1, \ldots, \Delta Y_i + \varepsilon_i, \ldots, \Delta Y_n + \varepsilon_n) = f_i(\Delta Y_1, \ldots, \Delta Y_i, \ldots, \Delta Y_n) + \varepsilon_1 \left.\frac{\partial f_i}{\partial(\Delta Y_1)}\right|_{\varepsilon=0} + \varepsilon_2 \left.\frac{\partial f_i}{\partial(\Delta Y_2)}\right|_{\varepsilon=0} + \cdots . \tag{A10}$$

Here, $|_{\varepsilon=0}$, means that all the ε_i are to be set equal to zero in the derivative $\partial f_i/\partial(\Delta Y_j)$. Carrying this out for Equation (A9) yields, after a little algebra,

$$f_i(\Delta Y + 0) = \varepsilon_1 M_{i1} + \varepsilon_2 M_{i2} + \cdots + \varepsilon_i M_{ii} + \cdots + \varepsilon_n M_{in}, \tag{A11}$$

where

$$f_i(\Delta Y + 0) \equiv \frac{\Delta Y_i}{\Delta t} - \sum_j \lambda_j^{(i)}(X_j + \Delta Y_j) - \sum_{j \geqslant k} [j, k]^{(i)}(X_j + \Delta Y_j) \times (X_k + \Delta Y_k) - \sum_{j \geqslant k \geqslant l} [j, k, l]^{(i)}(X_j + \Delta Y_j) \times (X_k + \Delta Y_k)(X_l + \Delta Y_l) \tag{A12}$$

and

$$M_{ij} = -\frac{\delta_{ij}}{\Delta t} + \lambda_j^{(i)} + \sum_k [j, k]^{(i)}(X_k + \Delta Y_k) + \sum_{k \geqslant l} [j, k, l]^{(i)}(X_k + \Delta Y_k)(X_l + \Delta Y_l). \tag{A13}$$

For all of the constituents we will have a linear system of n simultaneous algebraic equations for the ε_i.

$$\begin{aligned}
f_1(\Delta Y + 0) &= \varepsilon_1 M_{11} + \varepsilon_2 M_{12} + \varepsilon_3 M_{13} + \cdots + \varepsilon_j M_{1j} + \cdots + \varepsilon_n M_{1n}, \\
f_2(\Delta Y + 0) &= \varepsilon_1 M_{21} + \varepsilon_2 M_{22} + \varepsilon_3 M_{23} + \cdots + \varepsilon_j M_{2j} + \cdots + \varepsilon_n M_{2n}, \\
&\vdots \\
f_j(\Delta Y + 0) &= \varepsilon_1 M_{j1} + \varepsilon_2 M_{j2} + \varepsilon_3 M_{j3} + \cdots + \varepsilon_j M_{jj} + \cdots + \varepsilon_n M_{jn}, \\
&\vdots \\
f_n(\Delta Y + 0) &= \varepsilon_1 M_{n1} + \varepsilon_2 M_{n2} + \varepsilon_3 M_{n3} + \cdots + \varepsilon_j M_{nj} + \cdots + \varepsilon_n M_{nn}.
\end{aligned} \tag{A14}$$

After computing the $f_i(\Delta Y+0)$ and M_{ij} from Equations (A12) and (A13) the n ε_i may be solved for by matrix inversion and the initial guesses, ΔY_i, corrected, $\Delta Y_i^{(1)} = \Delta Y_i + \varepsilon_i$. These corrected guesses, $\Delta Y_i^{(1)}$, may then be used in the same procedure to calculate a new set of errors, $\varepsilon_i^{(1)}$, and the whole process repeated again. Presumably after an infinite number of iterations the trial values $\Delta Y_i^{(N)}$ will converge to the actual differencing values ΔX_i; i.e. $\lim_{N\to\infty} \Delta Y_i^{(N)} = \Delta X_i$ where $\Delta Y_i^{(N)} = \Delta Y_i^{(N-1)} + \varepsilon_i^{(N-1)}$. Because computing machines have finite accuracy, however, the calculated errors will never vanish. For the IBM 360, which does arithmetic to 14 places, the iterations were assumed to have converged when all the calculated percent errors were equal to or less than 10^{-14}, i.e. when

$$\frac{\varepsilon_i^{(n)}}{\Delta Y_i^{(n)}} \leqslant 10^{-14}. \tag{A15}$$

At the end of the iterations in a time step all the abundances are updated and the calculation proceeds to the next time step and another sequence of iterations.

For starting values in Equations (A14), those generated by the first order approximation method, described earlier, were used. Our experience with this has been that these initial guesses never differed by more than 5% from the final results and it never took more than 5 iterations to converge to the limit of machine accuracy. This method was tested against a zeroeth order technique, which, while more accurate, was 1000 times slower. The results of the two approaches always agreed to 3 or 4 places of accuracy over extended periods of time. While no serious attempt was made to establish criteria for absolute convergence or stability, it is our feeling that the scheme outlined here is consistent with the better understood numerical techniques, while being decidedly faster.

Acknowledgements

This work has been supported in part by the U.S. Atomic Energy Commission and the National Aeronautics and Space Administration. We are indebted to Dr. J. W. Truran for his continuing interest and advice on almost all aspects of this work. We wish to thank Dr. Len Rosen for many illuminating discussions and to Dr. Robert Jastrow, we would like to express our gratitude for his hospitality in making the facilities of the Goddard Institute for Space Studies available to us.

References

Aller, L. H.: 1961, *The Abundance of The Elements*, Interscience Publishers, New York, Ch. 10.
Arnett, W. D.: 1966, *Can. J. Phys.* **44**, 2533.
Arnett, W. D.: 1967, *Can. J. Phys.* **45**, 1621.
Arnett, W. D.: 1968, *Astrophys. J.* **153**, 341.
Arnett, W. D.: 1969, *Astrophys. J.* **157**, 1369.
Arnett, W. D. and Cameron, A. G. W.: 1967, *Can. J. Phys.* **45**, 2953.
Colgate, S. A.: 1968, *Astrophys. J.* **153**, 335.
Colgate, S. A.: 1970, Talk, given at the Goddard Institute for Space Studies, New York, January 1970.
Colgate, S. A. and White, R. H.: 1966, *Astrophys. J.* **143**, 626.
Delano, M. D.: 1969, Ph.D. thesis, New York University, unpublished.
Delano, M. D.: 1970, *Phys. Rev.* **A1**, 1175.
Hoyle, F.: 1946, *Monthly Notices Roy. Astron. Soc.* **106**, 343.
Hoyle, F. and Fowler, W. A.: 1960, *Astrophys. J.* **132**, 565.
Schwartz, R. A.: 1966, Ph.D. thesis, Columbia University, unpublished.
Schwartz, R. A.: 1967, *Ann. Phys.* **43**, 42.
Seeger, P. A., Fowler, W. A., and Clayton, D. C.: 1965, *Astrophys. J. Suppl.* **11**, No. 97.
Truran, J. W.: 1967, Private communication at the 'Summerset'.
Truran, J. W., Arnett, W. D., Tsuruta, S., and Cameron, A. G. W.: 1968, *Astrophys. Space Sci.* **1**, 129.
Wagoner, W. V.: 1968, *Astrophys. J. (Letters)* **151**, L103.
Wagoner, W. V.: 1969, *Astrophys. J. Suppl.* **18**, 247.